RSC Advances

ROYAL SOCIETY OF CHEMISTRY

www.rsc.org/advances

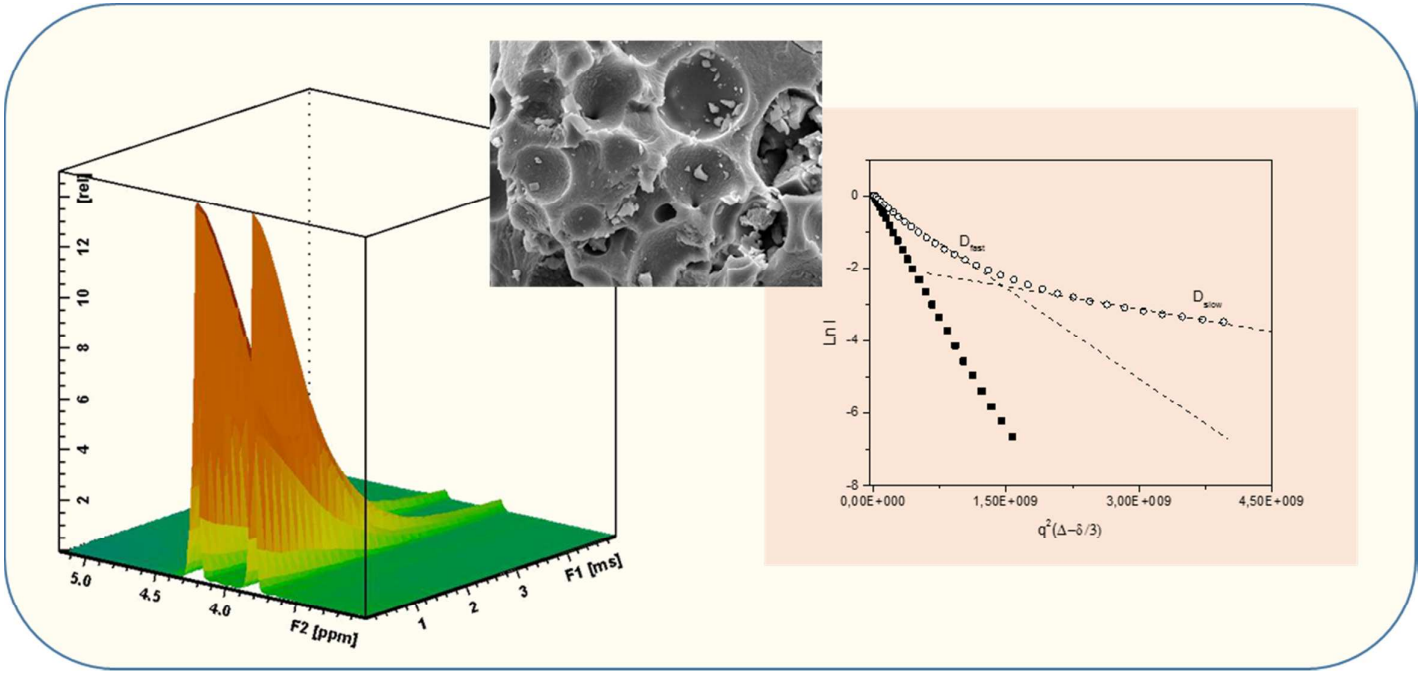

Assessing the diffusion of solvent and reaction species within a sol-gel matrix using Pulsed Field Gradient Spin Echo HR-MAS NMR

Journal Name

RSCPublishing

ARTICLE

Assessing diffusion in enzyme loaded sol-gel matrices

Cite this: DOI: 10.1039/x0xx00000x

Gustavo Barreira,[a] Ana S.D. Ferreira,[a,b] Pedro Vidinha,[a,c] Joaquim M.S. Cabral,[d] José M.G. Martinho,[e] João Carlos Lima,[a] Eurico J. Cabrita,[a]* Susana Barreiros[a]*

Received 00th January 2012,
Accepted 00th January 2012

DOI: 10.1039/x0xx00000x

www.rsc.org/

Pulsed Field Gradient Spin Echo High Resolution Magic Angle Spinning Nuclear Magnetic Resonance spectroscopy is a powerful technique to characterize confined biosystems. We used this approach to assess the diffusion of solvent and reaction species within sol-gel matrices differing in enzyme loading.

Introduction

Biocatalysis is an environmentally friendly alternative to chemical synthesis for many industrial applications ranging from the production of commodity chemicals to pharmaceutical compounds[1–3]. Enzyme immobilization is usually required for enzyme reuse and stabilization[4,5]. Sol-gel matrices are porous, chemically inert, thermally stable materials formed through the hydrolysis and condensation of metal alkoxides. They have been used extensively in the design of bioreactors, biosensors or artificial organs[6–9]. As the biocatalyst is added at the early stage of matrix formation, it is trapped within a cage[10] that prevents leaching while ensuring adequate access of substrates and release of products. Silica has been widely used for bioencapsulation, but more recently materials such as metallic particles and metal oxides have been used as well[11-13].

Possible restrictions on the diffusion of reacting species to and from the entrapped enzyme is an intuitive, common argument[4]. It has been shown early on that the specific activity of a sol-gel entrapped lipase increased asymptotically as enzyme loading approached zero[14]. The authors rationalized their finding on the basis of diffusional limitations of the substrate entry to or into the catalyst particles, mentioning also that aggregation of the enzyme might occur at high concentrations, resulting in a lower degree of dispersion in the sol-gel matrix.

Here we report on the assessment of diffusion in enzyme loaded sol-gel matrices using Pulsed Field Gradient Spin Echo (PFGSE) High Resolution Magic Angle Spinning (HR-MAS) Nuclear Magnetic Resonance (NMR) spectroscopy. HR-MAS NMR can be considered a hybrid between solid and solution state NMR, where the samples are spun at the magic angle[15,16]. This allows for the study of heterogeneous samples and semi-solid materials[17–19]. The application of PFGSE HR-MAS NMR to the study of sol-gel materials is largely an unexplored field. However, it allows the study of solvent/solute accessibility in sol-gel materials at experimental conditions relevant to sol-gel process optimization[20,21]. To the best of our knowledge, this is the first time that this approach is used to characterize sol-gel matrices with an immobilized biocatalyst. We also used fluorescence anisotropy spectroscopy to look at the effect of enzyme loading on the packing of entrapped enzyme molecules.

Experimental

Materials

Fusarium solani pisi cutinase was produced by an *Escherichia coli* WK-6 (a gift from Corvas International, Ghent, Belgium) and purified at IBB/IST[22,23]. High purity *(R,S)*-2-phenyl-1-propanol, *(R,S)*-2-phenyl-1-propyl butyrate, tetramethoxysilane (TMOS) and polyvinyl alcohol (PVA; MW 15.000) were from Sigma-Aldrich, *n*-butyltrimetoxysilane (BTMS) from Polysciences Inc., vinyl butyrate from Fluka, *n*-hexane and tridecane from Merck, Hydranal Coulomat A and C Karl-Fischer reagents from Metrohm, Polygoprep silica particles were from Macherey-Nagel.

Immobilization of cutinase in sol-gel matrices

Following our previous studies[24], we immobilized cutinase in 1:5 tetramethoxysilane (TMOS)/*n*-butyltrimetoxysilane (BTMS) sol-gel matrices. A typical procedure[24] consisted in preparing separately an aqueous solution containing the enzyme (265 μL of cutinase solution, plus 58 μL of 1 M NaF solution, plus 116 μL of 4 % w/v PVA solution - total of 24.36 mmol of water) and a mixture of precursors (76 μL of TMOS plus 487 μL of BTMS, yielding a 1:5 TMOS:BTMS molar ratio and a water/silane molar ratio = 8), adding the latter to the former under vigorous shaking on a vortex mixer until the mixture became homogeneous. It was then placed in an ice bath and kept there for 10 min while gelation took place, after which it was kept at 4 ºC for 24 h, followed by air drying at 35 ºC for 24 h.

The resulting xerogel was grinded and washed with aqueous buffer, acetone, and finally *n*-hexane. This procedure leads to average immobilization yields of ca. 90 %. Enzyme particle sizes averaged (120±40) μm.

Transesterification activity assays

Reactions – the transesterification of vinyl butyrate (300 mM) by *(R,S)*-2-phenyl-1-propanol (100 mM) – were performed in *n*-hexane, in glass vials (reaction volume of 2 mL) placed in a constant temperature (22 ºC) orbital shaker set for 400 rpm. Ester addition marked the start of reaction. The substrates and the solvent were dried with molecular sieves. Tridecane (20 mM) was used as external standard for GC analysis. For reutilization assays, the liquid medium was pipetted out at the end of reaction and fresh *n*-hexane was added to the sol-gel powder. After 24 h at room temperature, the solvent was removed and the sol-gel powder was dried for 24 h in an oven kept at 40 ºC, before being weighed and assayed again for enzyme activity.

Transesterification reaction analysis

Reaction conversion was measured by GC analysis performed with a Trace 2000 Series Unicam gas chromatograph equipped with a 30m x 0,32 mm i.d. fused silica capillary column coated with a 0.25 μm thickness film of 20% 2,3-dimethyl-6-tert-butyldimethylsilyl-β-cyclodextrin dissolved in BGB-15, from Analytik AG. Oven temperature program: 60-180 ºC ramp at 4 ºC min^{-1}, 180-220 ºC ramp at 10 ºC min^{-1}, and holding at 220 ºC for 5 min. Injection temperature: 250 ºC. Flame ionization detection (FID) temperature: 250 ºC. Carrier gas: helium (2.0 cm^3 min^{-1}). Split ratio: 1:20. No products were detected in assays carried out without enzyme. The initial rates given (per mg of protein) are the average of at least two measurements.

HR-MAS NMR diffusion spectroscopy

The sol-gel matrix was grinded in a mortar and loaded into a 12 μL, 4 mm ZrO_2, HR-MAS rotor. Neat *n*-hexane, a solution of 2-phenyl-1-propanol (2F1P; 100 mM) in *n*-hexane, a solution of the reaction product 2-phenyl-1-propyl butyrate (2F1P-butyrate; 100 mM) in *n*-hexane, or a solution of 2F1P and 2F1P-butyrate in *n*-hexane (100 mM in each species) was added to the rotor and the sample was allowed to swell for at least one hour before performing the NMR experiments. The Polygoprep® samples were prepared by loading the silica phases as supplied into a 12 μL, 4 mm ZrO_2, HRMAS rotor, and doing as described above for sol-gel matrices. All NMR experiments were performed using a Bruker Avance III 400 operating at 400.15 MHz for protons, equipped with a 4 mm high-resolution solid-state Magic Angle Spinning (MAS) probe and with a pulsed field gradient unit, capable of producing magnetic field pulsed gradients in the z-direction of 0.54 T m^{-1}. Samples were spun at the magic angle at a rate of 4 kHz. The experimental temperature determined under these conditions was 25 ºC and was constant within ± 0.1 ºC, as measured using the spectrometer thermocouple system. Diffusion measurements were performed using the stimulated echo sequence using bipolar sine gradient pulses and eddy current delay before the detection[25]. Typically, in each experiment 32 spectra of 32 K data points were collected, with values for the duration of the magnetic field pulse gradients (δ) of 1.0 to 3.0 ms, diffusion times (Δ) of 50 to 1000 ms, and an eddy current delay set to 5 ms. The gradient recovery time was 200 μs. The sine shaped pulsed gradient (g) was incremented from 5 to 95 % of the maximum gradient strength in a linear ramp. The diffusion coefficient is normally determined from the attenuation of the echo amplitude (I), according to:

$$I = I_0 \exp\left(-\gamma^2 g^2 \delta^2 D\left(\Delta - \frac{\delta}{3}\right)\right) = I_0 \exp\left(-q^2 D\left(\Delta - \frac{\delta}{3}\right)\right) \quad (1)$$

where γ denotes the gyromagnetic ratio, D the self-diffusion coefficient, and q^2 the product ($\gamma^2 g^2 \delta^2$). In heterogeneous systems, the displacement of the diffusing species depends on interactions with the porous matrix and may be restricted by pore walls. In this case, different regions can be distinguished depending on the size relations of the barriers, the duration of the gradient pulse, and the interval between the gradient pulses[26,27]. Generally in heterogeneous systems, the spin–echo attenuation deviates from the mono-exponential behaviour described by equation 1 because various diffusion domains may occur[28]. To determine the diffusion coefficients, the spectra were first processed in the F2 dimension by standard Fourier transform and baseline correction with the Bruker Topspin software package (version 3.1). The diffusion coefficients are calculated by exponential or bi-exponential fitting of the data belonging to individual columns of the 2D matrix using the Origin 9.0 data software program. At least two different measurements were done to determine each diffusion coefficient, whenever possible by measuring the signal intensity at more than one resonance in the spectra. The standard deviations of replicate measurements were below 6%. All the errors given throughout the text are the standard deviations of the exponential fitting. Proton NMR spectra are given in the ESI.

Fluorescence anisotropy decays

Time-resolved pico-second fluorescence measurements were performed using the single-photon counting timing method with laser excitation. The setup consisted of a mode-locked Spectra-Physics Vanguard 2000-HM532 Nd:YVO4 diode laser, delivering 2 Wof 533 nm light at a repetition rate of 76 MHz and pulse duration of ≈12 ps that synchronously pumped a cavity dumped 710-2 dye (rhodamine 6G) laser, delivering 3-4 ps pulses at a repetition rate of 1.9 MHz. The laser light was frequency doubled using an LBO crystal to obtain laser light of 280 nm used for excitation. Intensity decay measurements were made by an alternate collection of impulse and decay, with the emission polarizer set at the magic angle position. Impulse was recorded slightly away from the excitation wavelength with a scattering suspension. For the decays a cutoff filter was used, effectively removing all excitation light. The polarized decays were measured by alternate collecting of the horizontal and vertical components in successive cycles of 30 s until the number of counts at the maximum of the vertical component reached 20.000 counts. The global time of acquisition for each component was rigorously equal. The time per channel was 19.5 ps

and the number of channels used in the multichannel analyzer was 1024. The emission signal was first passed through a depolarizer, and then sent to a Jobin-Yvon HR320 monochromator with a grating of 100 lines/nm, and was recorded on a Hamamatsu 2809U-01 micro-channel plate photomultiplier as a detector. The instrument response function had an effective fwhm of 35 ps. The numerical aperture for fluorescence collection was 0.18 (lens with a diameter of 18 mm and a focal length of 50 mm); hence the half-angle θ was 10.4°, and paraxial conditions hold. The effect of a finite collection cone on the measured anisotropy was negligible[29]. The anisotropy decay curves were constructed from the I_{VV} (t), I_{VH}(t) fluorescence decays obtained with vertical polarized excitation light and selecting the vertical (I_{VV}(t)) or horizontal (I_{VH}(t)) components of the fluorescence, where $G=I_{HV}(t)/I_{HH}(t)$ is an experimental correction factor that considers the artifacts introduced by the detecting system on the polarized fluorescence light components:

$$r(t)=\frac{I_{VV}(t)-GI_{VH}(t)}{I_{VV}(t)+2GI_{VH}(t)} \quad (2)$$

For our experimental setup, G=1, because the polarized fluorescence light was depolarized before the entrance slit of the monochromator. The anisotropy fluorescence decays could be fitted by a sum of a one exponential decay plus a constant that considers the residual anisotropy:

$$r(t)=\beta_1 \exp(-t/\theta)+\beta_\infty \quad (3)$$

Assuming that cutinase is immobilized in the pores, the tryptophan fluorescence anisotropy results can be interpreted in the context of the wobbling-in-a-cone model which considers that tryptophan undergoes a restricted non-isotropic motion, wobbling around an axis within a cone characterized by a certain semi-angle and correlation time, θ:

$$r(t)=r(0)x\left[(1-S^2)\exp(-t/\theta)+S^2\right] \quad (4)$$

S is a generalized order parameter reflecting the degree of orientational constraint imposed by the surroundings. If the motion is isotropic, S = 0, and if it is completely restricted, S=1[30,31].

Results and discussion

In earlier works[24,32] we characterized TMOS/BTMS matrices as regards porosity, external morphology, and structure, the latter through diffuse reflectance infrared Fourier transform (DRIFT) spectroscopy and by solid-state ^{29}Si and ^{1}H NMR. In the course of these studies, we found that changing enzyme loading in the range 1.4-3 % did not have a marked effect on the specific activity of the enzyme. We now focused on lower enzyme loadings. Figure 1 shows results obtained for sol-gel entrapped cutinase up to the 6th utilization. As expected, enzyme activity remained fairly constant during the reutilization cycle period. The impact of enzyme loading on the specific activity of the enzyme was very modest for enzyme loadings above 1.5 %, but was very pronounced for values of the latter parameter below 0.5 %, similarly to what was observed by Reetz *et al*[14].

We had seen that grinding TMOS/BTMS matrices with an average enzyme loading of 1.4 % led to comparable initial reaction rates as for crushed supports[24], suggesting the absence of diffusional limitations. We now assessed diffusion in sol-gel matrices with both higher and lower enzyme loadings. Diffusion in heterogeneous samples can be determined by PFGSE NMR, as shown by Kärger *et al*.[27,33] for the study of diffusion in meso and nanoporous materials.

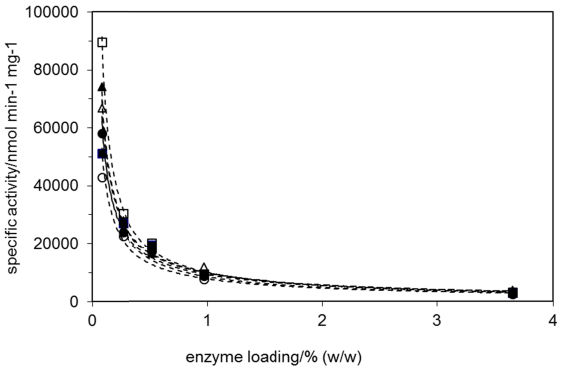

Fig 1 Impact of enzyme loading of sol-gel matrix on cutinase specific activity. Data given for five matrices with enzyme loadings of 0.08 %, 0.27 %, 0.52 %, 0.97 % and 3.65 % used six times consecutively in a transesterification reaction performed in *n*-hexane at room temperature, yielding the six data sets shown in the figure. ■, 1st; □, 2nd; ▲, 3rd; △, 4th; ●, 5th; ○, 6th. The lines are trendlines.

This methodology has also been applied under HR-MAS conditions to heterogeneous samples, allowing an increase in resolution since the use of MAS sharpens the usually broad NMR signals. We used PFGSE HR-MAS NMR to first determine self-diffusion coefficients in the absence of the sol-gel matrix. *N*-hexane (Figure 2a), as well as 2F1P and 2F1P-butyrate in *n*-hexane (see ESI), showed a linear correlation in the plot of ln I *vs.* $q^2(\Delta-\delta/3)$, as expected for a mono-exponential signal decay (equation 1). For *n*-hexane, the self-diffusion coefficient obtained by linear regression analysis was $(4.33\pm0.02)\times10^{-9}$ m^2 s^{-1}, in agreement with values in the literature[34] ranging from 4.00 to 4.28×10^{-9} m^2 s^{-1}. The presence of 2F1P (100 mM), with diffusion coefficient $(2.62\pm0.02)\times10^{-9}$ m^2 s^{-1}, did not affect the self-diffusion coefficient of *n*-hexane. In the presence of 2F1P-butyrate (100 mM), with diffusion coefficient $(2.34\pm0.02)\times10^{-9}$ m^2 s^{-1}, we observed a slight decrease in the self-diffusion coefficient of *n*-hexane $(3.89\pm0.02)\times10^{-9}$ m^2 s^1. The same effect was found for 2F1P. The observed impact on the diffusion of

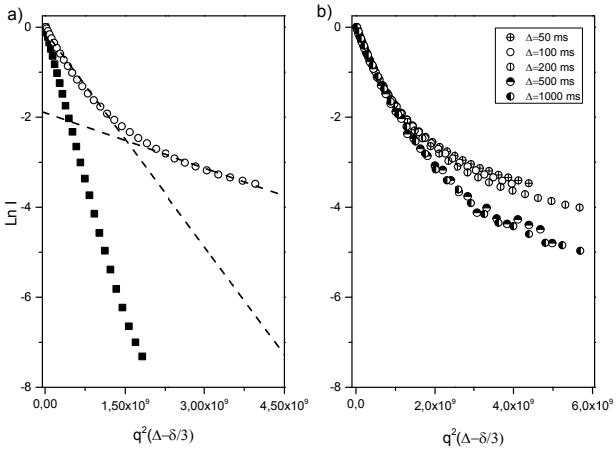

Fig 2 - Echo amplitude *vs.* $q^2(\Delta-\delta/3)$ for neat *n*-hexane (■) and for *n*-hexane in the presence of the sol-gel matrix (other symbols), for Δ=100 ms (○), as shown in (a), and for different diffusion times (b).

n-hexane and 2F1P indicates that the presence of 2F1P-butyrate brings about a slight increase in the viscosity of the solution.

PFGSE HR-MAS NMR was then used to determine the diffusion coefficient of *n*-hexane in the presence of the matrix. As shown in Figure 2a, the deviation from linearity observed for the echo amplitude of *n*-hexane in the matrix is a clear indication of multi-exponential behavior. The simplest diffusion model to explain these results considers two diffusion domains, one inside the pores of the matrix and another outside, leading to a bi-exponential decay. In the case of slow exchange between the two domains ($\Delta \times k_{exch} < 0.1$), a bi-exponential echo decay will be observed with each domain possessing its own diffusion coefficient D_i, with the fraction of molecules in each domain expressed as p_i:

$$\frac{I}{I_0} = \sum_{i=1}^{n} p_i \exp\left(-q^2 D_i\left(\Delta - \frac{\delta}{3}\right)\right) \quad (5)$$

This model is dependent on several parameters, such as the distribution of populations of molecules in the two environments, the diffusion coefficients in each environment, and the exchange rate between the two sites. The shape of the plot observed in Figure 2 is determined by all those parameters. However, on a qualitative basis, the plot obtained for *n*-hexane in the presence of the matrix can be rationalized by a model where the molecules undergo a slow exchange process between the two sites, as described by Johnson[35] and Cabrita *et al.*[36]. These two sites correspond to a slow diffusion environment (D_{slow}) inside the pores and a fast diffusion path (D_{fast}) outside the matrix. The slopes of the linear regression in Figure 2a represent approximately the two diffusion domains. Confirmation that the bi-exponential behavior of the echo amplitude is due to chemical exchange phenomena was obtained by performing different PGSE measurements with increasing diffusion times (Figure 2b). Changes in the latter parameter are accompanied by changes in the behavior of the echo amplitude when the relation between the observation time (diffusion time) and the residence time in the diffusion domains is altered in each experiment. For longer diffusion times, there is a tendency for mono exponential behavior as the condition of fast exchange in the diffusion domain ($\Delta \times k_{exch} > 10$) is approached[35,36].

To ensure that D_{fast} and D_{slow} determined in the sol-gel matrix reflect the inter and intraparticular nature of the diffusion, we performed independent HRMAS diffusion experiments using Polygoprep silica particles with the same particle size (63-200 μm) but two different pore sizes (60 and 100 Å) (Figure 3). The figure shows a bi-exponential behaviour of *n*-hexane diffusion, similar to that observed in the sol-gel matrices. It is clear that D_{fast} is almost not affected by pore size in the range of pore sizes studied. On the other hand, D_{slow} is substantially affected by pore size, its value increasing with increasing pore size, as might be expected.

To characterize the transport properties of the reaction species within the matrix, we performed experiments with individual solutions of 2F1P and 2F1P-butyrate in *n*-hexane. For both solutions, the echo amplitude of *n*-hexane shows a bi-exponential behaviour. However, differences were found for 2F1P and 2F1P-butyrate. While 2F1P shows a clear bi-exponential behaviour, the data for 2F1P-butyrate is well fitted by a mono-exponential (see ESI). The differences in the behaviour of the attenuation of the echo amplitude

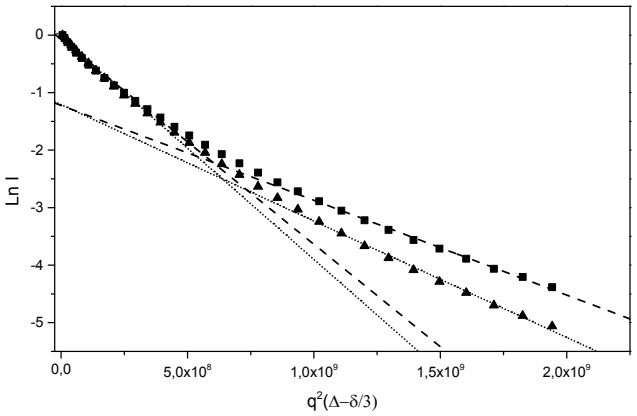

Fig 3 Echo amplitude *vs.* $q^2(\Delta-\delta/3)$ for *n*-hexane in Polygoprep® silica phases with the same particle size (63-200 □m), for Δ=100 ms. (■), Particles with 60 Å pore size. § , Particles with 100 Å pore size.

are due to different exchange regimes between diffusion domains for the two species. For the diffusion times sampled, the bi-exponential behaviour of *n*-hexane and 2F1P denotes a slow exchange process between the inter and intraparticular domains of the matrix, allowing the determination of D_{fast} and D_{slow}, and respective populations (Table 1), while the mono-exponential attenuation of 2F1P-butyrate is due to a fast exchange regime. However, the low value obtained for the diffusion coefficient of 2F1P-butyrate in the presence of the matrix - $(0.52\pm0.01)\times10^{-9}$ m^2 s^1 - when compared to the one obtained without support - $(2.34\pm0.02)\times10^{-9}$ m^2 s^{-1} - indicates that 2F1P-butyrate must have a high population inside the matrix. The reason for the differences in the exchange regime of the two compounds must originate in the nature of their interactions with the support. Despite these differences, in the presence of the matrix, the effect of 2F1P or 2F1P-butyrate in the diffusion of *n*-hexane is similar to that observed in the absence of support, *i.e.* only 2F1P-butyrate has a significant effect on the diffusion coefficient of the solvent, which decreases (see ESI). As for the effect of the two reaction species when they are in solution together in the presence of the matrix, peak overlap (see ESI) precludes an accurate determination of the diffusion coefficients of 2F1P and 2F1P-butyrate.

Since 2F1P shows a slow exchange regime and is the relevant reaction species to analyse initial reaction rate data, it was chosen to determine the effect of the enzyme on transport properties within the matrix. The results obtained for the echo amplitude of *n*-hexane and 2F1P in the presence of the sol-gel matrix without enzyme or loaded with 1 % of cutinase are shown in Figure 4. The slopes corresponding to the slow and fast component of the curves were included for comparison. *N*-hexane and 2F1P show a bi-exponential behaviour whether the matrix has enzyme or not. Table 1 gives the values obtained for the self-diffusion coefficients and respective populations

derived from the bi-exponential fitting, using the sol-gel matrices loaded with 0.5 %, 1.0 % and 2.5% of cutinase. The self-diffusion coefficients obtained for *n*-hexane and 2F1P, both for the fast and for the slow diffusion component, are very similar, independently of the conditions studied. The small differences found in the presence and in the absence of enzyme do not justify loss of enzyme specific activity due to diffusional restraints.

Table 1 Self-diffusion coefficients, D_i, and respective populations, p_i, determined by HR-MAS PFGSE NMR. 2F1P stands for the substrate 2-phenyl-1-propanol.

			Diffusion coefficient ($\times 10^{-9}$ m^2s^{-1})*			
			D_{fast}	D_{slow}	p_{fast}	p_{slow}
n-hexane		Matrix	2.73 ±0.04	0.53 ±0.02	0.80 ±0.01	0.20 ±0.01
		Matrix, with 0.5% enzyme	2.46 ±0.03	0.51 ±0.02	0.81 ±0.01	0.19 ±0.01
		Matrix with 1.0% enzyme	3.22 ±0.05	0.35 ±0.02	0.82 ±0.01	0.18 ±0.01
		Matrix with 2.5% enzyme	2.21 ±0.04	0.64 ±0.04	0.79 ±0.02	0.21 ±0.02
n-hexane +2F1P	*n*-hexane	Matrix	2.86 ±0.06	0.56 ±0.03	0.76 ±0.01	0.24 ±0.01
		Matrix with 0.5% enzyme	3.06 ±0.04	0.89 ±0.03	0.74 ±0.01	0.26 ±0.01
		Matrix with 1.0% enzyme	2.53 ±0.02	0.25 ±0.01	0.80 ±0.01	0.20 ±0.01
		Matrix with 2.5% enzyme	2.85 ±0.06	0.70 ±0.06	0.83 ±0.02	0.17 ±0.02
	2F1P	Matrix	2.48 ±0.08	0.36 ±0.01	0.52 ±0.01	0.48 ±0.01
		Matrix with 0.5% enzyme	1.76 ±0.02	0.27 ±0.01	0.58 ±0.01	0.42 ±0.01
		Matrix with 1.0% enzyme	1.92 ±0.09	0.32 ±0.05	0.70 ±0.03	0.30 ±0.04
		Matrix with 2.5% enzyme	1.7 ±0.1	0.23 ±0.01	0.68 ±0.04	0.32 ±0.04

*The errors represent the standard deviation of the exponential fitting performed to compute the diffusion.

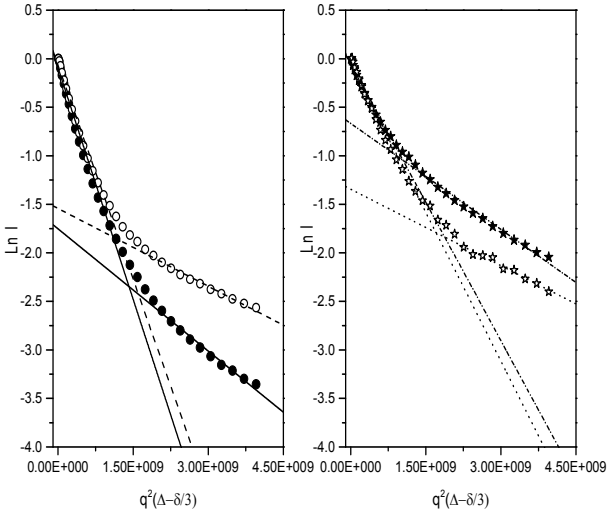

Fig 4 Echo amplitude *vs.* $q^2(\Delta-\delta/3)$ for *n*-hexane and for 2F1P in *n*-hexane, in the presence of the sol-gel matrix without enzyme (○ hexane, ☆ 2F1P) and in the presence of the sol-gel matrix loaded with 1 % of cutinase (● hexane, ☆ 2F1P), for Δ=100 ms.

Table 1 includes the population for each diffusion domain derived from the data. While the distribution of *n*-hexane between diffusion domains remains more or less constant, for matrices with enzyme loadings of 1 % and higher there is a decrease in the 2F1P population associated to the pores of the matrix. A possible explanation might be a change in the affinity of the matrix for 2F1P. Assuming that the total number of silanol groups is constant, and taking into account that one enzyme molecule has many residues that are able to establish interactions with silanol groups, in enzyme loaded matrices there would be less silanol groups free to interact with 2F1P inside the pores.

Fluorescence anisotropy spectroscopy is based on the fact that a fluorophore excited by polarized light also emits polarized light, whose intensity at a different direction from that of the incident light over a period of time will depend on the mobility of the fluorophore [30,31]. Cutinase has only one tryptophan residue, diametrically opposite to the active site (Trp-69), whose fluorescence emission can be selectively measured by choosing an appropriate wavelength of excitation[37,38]. A fast increase in the fluorescence emission intensity of the tryptophan residue along a plane perpendicular to that of the exciting light indicates that the region where the tryptophan residue is located is relatively free to tumble[39,40].

To verify the impact of enzyme loading on the packing of cutinase inside the sol-gel matrices, as might be caused by enzyme aggregation, fluorescence anisotropy decays were measured at different enzyme loadings (Figure 5). Table 2 summarizes the results obtained for the fitting of the tryptophan fluorescence anisotropy decays by equation 3. The anisotropy at time zero is around 0.3, which is slightly higher than the typical value for tryptophan in solution and in proteins (~0.25)[39] but lower than the theoretical

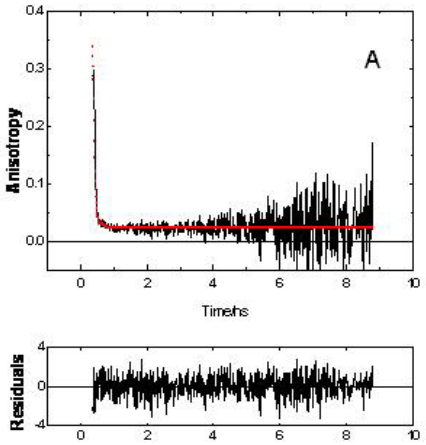

Fig 5 Time resolved anisotropy decay curve, r(t), of the single tryptophan residue of cutinase entrapped in a sol-gel matrix with 3.63 % enzyme loading, and the corresponding residual of the fitting by equation 3.

predicted value of 0.4 for collinear transition dipole moments for absorption and emission. The order parameter S^2 is low in all cases, due to depolarization of the tryptophan fluorescence at a rate much faster than the rotational constant of the protein. Thus although the order parameter shows a slight increase with enzyme loading, anisotropy cannot be used to conclude unequivocally on the aggregation state of entrapped cutinase.

Table 2 -Tryptophan fluorescence anisotropy correlation time, θ, pre-exponential factor, β_1, residual anisotropy, β_∞, and order parameter, S^2, at different cutinase loadings in the sol-gel matrices.

Enzyme loading %	β_1	θ (ps)	β_∞	S^2
3.63	0.30	2.9	0.022	0.068
1.60	0.34	4.8	0.009	0.029
0.06	0.32	5.5	0.006	0.020

Conclusions

The sol-gel process has been used extensively to generate bioactive materials for many applications. Optimization of the performance of these and other advanced materials requires detailed characterization of the entrapped biosystem, including accessibility of reaction species, which is usually lacking. The utility of PFGSE HR-MAS NMR spectroscopy for this type of characterization was demonstrated here through the assessment of the diffusion of solvent and reaction species in the presence of a sol-gel matrix with different enzyme loadings.

Acknowledgements

This work has been supported by Fundação para a Ciência e a Tecnologia (FCT/MEC) through projects/grants PEst-C/EQB/LA0006/2013, PTDC/QUI/64744/2006, SFRH/BD/34800/2007 (GB), SFRH/BPD/41546/2007 (PV) and SFRH/BPD/88144/2012 (ASDF), and by FEDER. The NMR spectrometers are part of the National NMR Network (RNRMN) and are funded by FCT/MEC (project RECI/BBB-BQB/0230/2012). We thank Prof. Luís Fonseca and Mário Fonseca for the production of cutinase, Marta Corvo for the acquisition of HR-MAS spectra, Dr. Alan Phillips for performing enzyme particle size measurements, and Macherey-Nagel for the gift of Polygoprep silica particles.

Notes and references

[a] REQUIMTE/CQFB, Departamento de Química, Faculdade de Ciências e Tecnologia, Universidade Nova de Lisboa, 2829-516 Caparica, Portugal
[b] Centro de Química Estrutural, Instituto Superior Técnico, Av. Rovisco Pais, 1049-001 Lisboa, Portugal
[c] Instituto de Química, Universidade de São Paulo, Av. Prof. Lineu Prestes, 748, CEP 05508-900, São Paulo, SP, Brasil.
[d] Department of Bioengineering and IBB - Institute for Biotechnology and Bioengineering, Instituto Superior Técnico (IST), Av. Rovisco Pais, 1049-001, Lisboa, Portugal
[e] Centro de Química-Física Molecular, Instituto Superior Técnico, Av. Rovisco Pais, 1049-001 Lisboa, Portugal
Electronic Supplementary Information (ESI) available: [details of any supplementary information available should be included here]. See DOI: 10.1039/b000000x/

1. U. T. Bornscheuer, G. W. Huisman, R. J. Kazlauskas, S. Lutz, J. C. Moore, and K. Robins, *Nature*, 2012, 485, 185–194.
2. T. Hudlicky and J. W. Reed, *Chem. Soc. Rev.*, 2009, **38**, 3117–3132.
3. C. Liese, A., Seelbach, K., Wandrey, *Industrial Biotransformations*, Wiley-VCH, 2nd edn., 2006.
4. U. Hanefeld, L. Gardossi, and E. Magner, *Chem. Soc. Rev.*, 2009, **38**, 453–468.
5. R. A. Sheldon, *Adv. Synth. Catal.*, 2007, **349**, 1289–1307.
6. D. Avnir, S. Braun, O. Lev, and M. Ottolenghi, *Chem. Mater.*, 1994, **6**, 1605–1614.
7. E. Ruiz-Hitzky, M. Darder, P. Aranda, and K. Ariga, *Adv. Mater.*, 2010, **22**, 323–336.
8. C. Sanchez, P. Belleville, M. Popall, and L. Nicole, *Chem. Soc. Rev.*, 2011, **40**, 696–753.
9. A. Sassolas, L. J. Blum, and B. D. Leca-Bouvier, *Biotechnol. Adv.*, 2012, 30, 489–511.
10. N. Nassif and J. Livage, *Chem. Soc. Rev.*, 2011, **40**, 849–859.
11. N. Nagai, Y. Suzuki, C. Sekikawa, T. Y. Nara, Y. Hakuta, T. Tsunoda, and F. Mizukami, *J. Mater. Chem.*, 2012, 22, 3234.
12. N. Steunou, C. Mousty, O. Durupthy, C. Roux, G. Laurent, C. Simonnet-Jégat, J. Vigneron, A. Etcheberry, C. Bonhomme, J. Livage, and T. Coradin, *J. Mater. Chem.*, 2012, **22**, 15291.
13. R. Andre, M. N. Tahir, F. Natalio, and W. Tremel, *FEBS J.*, 2012, **279**, 1737–49.

14. M. T. Reetz, a Zonta, and J. Simpelkamp, *Biotechnol. Bioeng.*, 1996, **49**, 527–34.

15. A. GARROWAY, AN (GARROWAY, *J. Magn. Reson.*, 1982, **49**, 168–171.

16. A. T. Townsend, R.R., Hotchkiss, *Techniques in Glycobiology*, M. Dekker, 1997.

17. L. R. Carvalho, M. C. Corvo, R. Enugala, M. M. B. Marques, and E. J. Cabrita, *Magn. Reson. Chem.*, 2010, 48, 323–330.

18. S. Viel, F. Ziarelli, and S. Caldarelli, *Proc. Natl. Acad. Sci. U. S. A.*, 2003, **100**, 9696–9698.

19. F. Ziarelli, L. Peng, C.-C. Zhang, and S. Viel, *J. Pharm. Biomed. Anal.*, 2012, 59, 13–17.

20. C. Johnson, *Prog. Nucl. Magn. Reson. Spectrosc.*, 1999, **34**, 203–256.

21. M. P. G. Lippens, M. Bourdonneau, C. Dhalluin, R. Warrass, T. Richert, C. Seetharaman, C. Boutillon, *Curr. Org. Chem.*, 1999, **3**, 147–169.

22. C. M. Carvalho, M. R. Aires-Barros, and J. M. Cabral, *Biotechnol. Bioeng.*, 1999, **66**, 17–34.

23. G. Lauwereys, M., de Geus, P., de Meutter, J., Stanssens, P., Matthyssens, in *Lipases: Structure, mechanism and genetic engineering*, ed. R. Alberghina, L., Schmid, R.D., Verger, GBF monogr., 1991, pp. 243–251.

24. P. Vidinha, V. Augusto, M. Almeida, I. Fonseca, A. Fidalgo, L. Ilharco, J. M. S. Cabral, and S. Barreiros, *J. Biotechnol.*, 2006, **121**, 23–33.

25. D. H. Wu, A. D. Chen, and C. S. Johnson, *J. Magn. Reson. Ser. A*, 1995, 115, 260–264.

26. J. Kärger, *Adv. Colloid Interface Sci.*, 1985, 23, 129–148.

27. R. Kärger, J., Valiullin, *Diffusion in Porous Media. eMagRes*, John Wiley & Sons, Ltd, 2011.

28. F. Stallmach, S. Gröger, V. Künzel, J. Kärger, O. M. Yaghi, M. Hesse, and U. Müller, *Angew. Chem. Int. Ed. Engl.*, 2006, **45**, 2123–2126.

29. T. J. V Prazeres, A. Fedorov, S. P. Barbosa, J. M. G. Martinho, and M. N. Berberan-Santos, *J. Phys. Chem. A*, 2008, **112**, 5034–5039.

30. G. Lipari and A. Szabo, *Biophys. J.*, 1980, **30**, 489–506.

31. E. L. Quitevis, A. H. Marcus, and M. D. Fayer, *J. Phys. Chem.*, 1993, **97**, 5762–5769.

32. P. Vidinha, S. Barreiros, J. M. S. Cabral, T. G. Nunes, a. Fidalgo, and L. M. Ilharco, *J. Phys. Chem. C*, 2008, **112**, 2008–2015.

33. D. N. Kärger, J., Ruthven, D.M., Theodorou, *Diffusion in Nanoporous Materials*, Wiley-VCH, 2012.

34. S. Viel, F. Ziarelli, G. Pagès, C. Carrara, and S. Caldarelli, *J. Magn. Reson.*, 2008, **190**, 113–123.

35. C. S. Johnson, *J. Magn. Reson. Ser. A*, 1993, **102**, 214–218.

36. E. J. Cabrita, S. Berger, P. Bräuer, and J. Kärger, *J. Magn. Reson.*, 2002, **157**, 124–131.

37. J. J. Prompers, C. W. Hilbers, and H. A. Pepermans, *FEBS Lett.*, 1999, **456**, 409–416.

38. P. C. Weisenborn, H. Meder, M. R. Egmond, T. J. Visser, and A. van Hoek, *Biophys. Chem.*, 1996, **58**, 281–288.

39. J. M. G. Martinho, A. M. Santos, A. Fedorov, R. P. Baptista, M. A. Taipa, and J. M. S. Cabral, *Photochem. Photobiol.*, 2003, **78**, 15–22.

40. A. M. Santos, A. Fedorov, J. M. G. Martinho, R. P. Baptista, M. A. Taipa, and J. M. S. Cabral, *J. Phys. Chem. B*, 2008, **112**, 3581–3585.